PHOTONICS Research

Vortex random fiber laser with controllable orbital angular momentum mode

Xiaoya Ma,[1] Jun Ye,[1] Yang Zhang,[1] Jiangming Xu,[1,2] Jian Wu,[1] Tianfu Yao,[1] Jinyong Leng,[1] and Pu Zhou[1,*]

[1]College of Advanced Interdisciplinary Studies, National University of Defense Technology, Changsha 410073, China
[2]e-mail: jmxu1988@163.com
*Corresponding author: zhoupu203@163.com

Received 27 October 2020; revised 14 December 2020; accepted 18 December 2020; posted 21 December 2020 (Doc. ID 413455); published 1 February 2021

In this paper, we propose and experimentally demonstrate a vortex random fiber laser (RFL) with a controllable orbital angular momentum (OAM) mode. The topological charge of the vortex RFL can range from −50 to 50 with nearly watt-level output power. A triangular toroidal interferometer is constructed to verify the spiral phase structure of the generated vortex random laser with a special coherence property. Vortex RFLs with fractional topological charge are also performed in this work. As the first demonstration of a vortex RFL with a controllable OAM mode (to the best of our knowledge), this work may not only offer a valuable reference on temporal modulation of a vortex beam and optical field control of an RFL but also provide a potential vortex laser source for applications in imaging, sensing, and communication.

https://doi.org/10.1364/PRJ.413455

1. INTRODUCTION

A vortex beam is a classic type of spatially structured light beam that shows a spiral wavefront with a centrally located phase singularity and carries an orbital angular momentum (OAM) of $l\hbar$ (l is the topological charge; $\hbar$ is the reduced Planck constant) per photon [1–4]. The current research of the vortex beam mainly addresses vortex generation [5–7], OAM manipulation [4,8], and special optical vortex [9,10]. Owing to these distinctive properties, vortex beams attracted much attention in optical communication [11,12] and optical tweezers [13] as soon as being discovered. In order to serve various demands of applications, spatial and temporal modulation such as the spatiotemporal coherence control of a vortex beam is creating extensive concern. Previous studies have shown that spatial coherence modulation makes vortices perform unique optical effects, which are different from those of conventional completely coherent vortices and extend a new branch called the "partially coherent vortex beam" [14,15]. Conspicuous behavior of a partially coherent vortex beam is that intensity distribution would be transformed from a hollow profile into a solid core along with degeneration of spatial coherence [10]. This effect can achieve Gaussian, flat, or hollow profiles of beam intensity easily via spatial coherence modulation, which allows a vortex beam to demonstrate great performance in particle trapping [16]. Moreover, the degree of spatial coherence of a partially coherent vortex beam is confirmed to be capable of self-reconstruction, further extending its applications in information transmission and recovery [10]. Practical applications such as free space optical communication may be challenged by atmospheric turbulence-like scintillation of light intensity, where a partially coherent vortex beam behaves better in decreasing scintillation than a partially coherent beam [17].

Up to now, most of the reported vortex fiber lasers have employed a defined cavity structure [18–20]. As we know, the demonstration of a cavity-structured fiber laser with stable temporal characteristics is, however, not trivial for the influence of a common self-pulsing factor [21–23]. Further, modulation of an obtained vortex fiber laser is difficult. Hence, a temporal stable laser source is crucial for the spatiotemporal modulation of a vortex fiber laser [24–27].

At this point, a temporally stable random fiber laser (RFL) could be a remarkable option for light sources to generate a vortex beam. As a new type of laser regime, an RFL employs Rayleigh scattering (RS) to provide randomly distributed feedback and stimulated Raman scattering (SRS) to realize power amplification [28,29]. Different from the rare-earth-doped fiber lasers, whose emission windows are located at several discrete wavebands, an RFL enabled by Raman gain in the passive fiber has become a ready-made and well-suited platform to obtain a wavelength-tunable output. Besides, low coherence of an RFL leads to weak speckle effect in imaging, which can generate vortex beams with more homogeneous intensity distribution and may be of great help for optical tweezers. The simple structure of an RFL also attracts great attention for its potential to

realize cost-effective practical applications. Due to these unique properties, RFLs have been widely used in optical communication [30,31], remote sensing [32], frequency conversion [33], and ultrafast lasing [34]. Since the first demonstration of an RFL, many efforts on power scaling [35–38], polarization [39,40], and spectral manipulation [41,42] have been made. As a significant manifestation, temporal property of an RFL has also been of great interest. Previously studies have demonstrated experimentally that, an RFL, especially if pumped by an amplified spontaneous emission (ASE) source [23], demonstrates ideal temporal stability with suppressed amplitude fluctuation, which allows an RFL to exhibit superior quality in various applications, such as midinfrared laser [43] and pulsing operation [44,45]. It is promising that the demonstration of a vortex RFL could incubate novel practical applications and further offer a platform for investigation of the vortex beam's temporal modulation and an RFL's optical field control.

In this paper, a vortex RFL with a controllable OAM mode has been proposed and experimentally realized for the first time to the best of our knowledge. Distinct spiral phase behaviors derived from an annular vortex beam with a dark hollow can be distinguished, and the topological charge of the vortex beam can range from −50 to 50 with nearly watt-level output power. Verification and wavefront analysis have been accomplished via a triangular toroidal interference setup; fractional phases are also performed, indicating that the generated vortex RFL can provide a potential source for many applications, such as imaging, sensing, and communication.

2. EXPERIMENTAL SETUP

To generate such vortex RFLs and realize optical field modulation, we design and construct an experimental setup, as schematically shown in Fig. 1. The RFL employs an all-fiber half-opened structure, which is composed of a 5 km long passive fiber (8 μm core diameter and 0.14 NA) providing Raman gain and randomly distributed feedback, along with a highly reflective fiber Bragg grating (FBG) centered at 1092.1 nm generating point feedback. The passive fiber and FBG are spliced with the common port and the 1090 nm port of a wavelength division multiplexer (WDM), respectively. The pump source centered at 1046 nm is spliced with the 1040 nm port of WDM. All the free fiber ends are 8° cleaved to suppress the parasitic feedback, and the random laser output is utilized as the illumination of the following vortex generation setup. The random lasing radiated from the passive fiber is collimated by a collimator and slashed by an aperture to apply a suitable size to the spatial light modulator (SLM, operating at 1000–1100 nm) before incident on the polarization beam splitter (PBS). After passing the PBS, the laser beam is separated into two parts. The reflective beam with vertical polarization is incident on a diffuser for elimination, and the other with horizontal polarization is transmitted directly for the following vortex conversion and interference. The SLM is mounted after the PBS, and real-time vortex spots are captured by a CCD camera after being focused by a convex lens, as shown in Fig. 1(a).

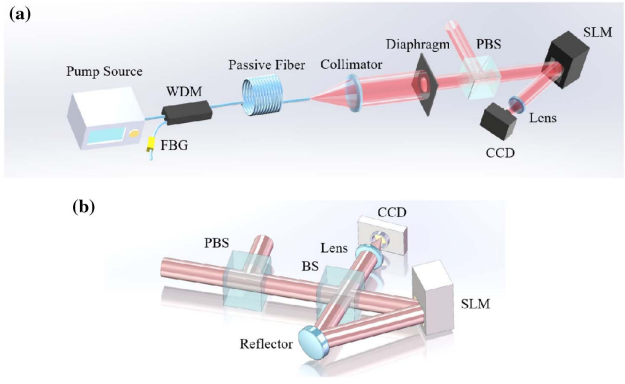

Fig. 1. Experimental setup of the vortex RFL system. (a) Generation setup of the vortex RFL. (b) Interference setup of the vortex RFL. WDM, wavelength division multiplexer; FBG, fiber Bragg grating with central wavelength at 1092.1 nm; PBS, polarization beam splitter; BS, beam splitter; SLM, spatial light modulator; CCD, charge-coupled device.

Figure 1(b) illustrates the interferometer with a triangular toroidal structure, formed by a beam splitter (BS), a reflector with the reflectivity >99.9% at 1000–1400 nm, and the SLM. In the transmissive path, the function of SLM is to manipulate the vortex RFL, while it is also utilized as a reflective mirror in the reflective path. After reconvergence inside the BS, the interference light is reflected, and real-time interferograms are captured by a CCD camera after being focused via a convex lens. By loading different holograms onto the SLM, the desired laser modes can be gathered.

3. EXPERIMENTAL RESULTS AND DISCUSSIONS

To analyze physical properties and verify the spiral wavefront of the generated vortex RFL, the output properties of the RFL are first characterized. The normalized amplitude spectra of a 1092.1 nm laser at different pump powers are shown in Fig. 2(a). It can be found that, owing to the utilization of FBG with a narrow reflection bandwidth, the full width at half maxima (FWHM) of the random lasing has no serious broadening after the pump power increases to 2.24 W, and the maximal FWHM is measured to be ∼0.38 nm. Figure 2(b) shows the power evolution curves of an RFL. Prior to 3.44 W pump power, the rising tendency of output power is relatively steep, which turns flat after exceeding the second-order Stokes threshold of 3.4 W. The maximal power of the random lasing measured at the end of the passive fiber is ∼1.04 W with the pump power of 4.5 W, corresponding to an optical–optical efficiency of ∼23%. Considering the losses induced by the spatial structure, such as the insertion loss of the lens and diaphragm, the reflected vertically polarized light of the PBS, and the limitation of effective illumination area of SLM, the maximal power at the point of CCD camera is ∼0.5 W.

Then, via loading holograms with different l as depicted in Fig. 3(a) on SLM [2,3,11], the vortex spots were obtained by the CCD camera with l (the topological charge) from 1 to 5 after being focused by a convex lens, as shown in Fig. 3(b). It can be seen that a dark hollow appears at the center of the vortex beam, indicating where the phase singularity exists. Except for the surrounding diffraction ripples, circinate and regular

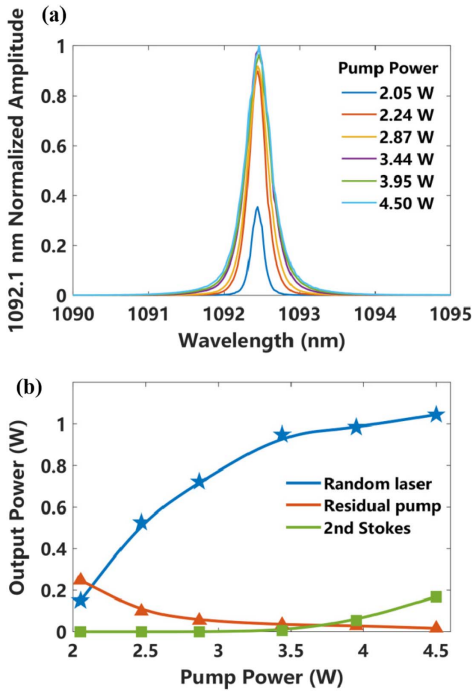

Fig. 2. (a) Normalized amplitude spectra of a 1092.1 nm random laser at different pump powers. (b) Output power evolution of RFL at different pump powers.

distribution of beam intensity with clear boundaries can be observed; further, the size of annulus expands as the topological charge grows.

To verify the spiral phase of generated vortex RFL, an interferometer is constructed. A matter to be aware of is that the coherence property of RFL has not been investigated systematically thus far, while it is a common view for researchers that the spatiotemporal coherence of a random laser is lower than that of a conventional laser, which enables an RFL to demonstrate better performance in many applications such as speckle-free imaging [46,47]. In this work, the temporal coherence plays a dominant role, as a passive fiber only supports two propagation modes in the wavelength range around 1090 nm, which is unsatisfied for the spatial coherence to be regarded. Besides, the real-time output spectra of an RFL are obtained in Ref. [48], and the average total spectrum can be seen as an intensity envelope with a wide bandwidth, which determines the temporal coherent length (about a few millimeters in this work). Therefore, it is difficult to employ the common parallelogram path, namely, the Mach–Zehnder (M–Z) interferometer, in regulating the optical path difference (OPD), where the incident beam is separated into two completely independent beams, and the interference performances are affected largely by the temporal coherence feature of the RFL. To address this challenge, we utilize a triangular loop [see Fig. 1(b)]. Two beams pass through three sides of the same triangle in the loop, consequently ensuring that OPD is strictly zero and even further simplifying the setup. The interference fringes of vortex RFL with l from 1 to 5 acquired by the CCD camera are shown in Fig. 3(c). It can be distinguished that the

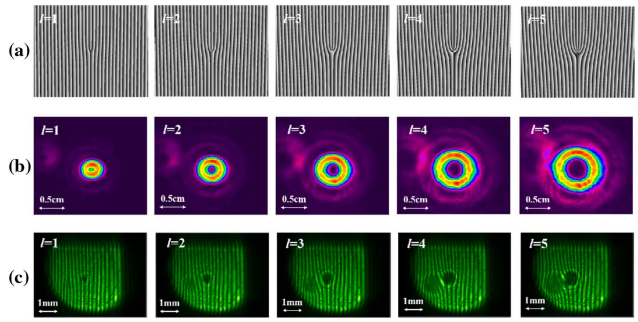

Fig. 3. (a) Holograms loaded onto the SLM. (b) Intensity distribution. (c) Interference fringes of the vortex RFL acquired by a CCD. The topological charge l is 1 to 5 from left to right.

generated interference fringes vanish at the center of each interferogram, where a phase singularity exists, and form a fork pattern located in the center. Further, the number of the disappeared fringes is the same as in the topological charge l. At this point, the validity and the spiral phase of vortex RFL generated above are confirmed.

A vortex RFL with negative OAMs has also been shown. Figure 4 exhibits vortex performances when reverse phases are loaded on the SLM. Compared with Fig. 3, vortex spots with l of −1 to −5, as shown in Fig. 4(b), manifest much the same as those with the positive l numbers; however, the orientation of fork fringes has a reverse rotation of 180°, as illustrated in Fig. 4(c).

In the experiment, phase distribution can be changed flexibly with the aid of SLM. The vortex performances with l of 10, 20, and 50 are exhibited as well, as depicted in Fig. 5. The size of annulus multiplies as l is increased twofold. Further, the intensity distribution gradually becomes dispersive with the range of surrounding diffraction ripples extending, whereas the beam spots remain rounded. Through observing the evolution of vortex spots with l from 1 to 50, it can be measured that the size of vortex spots is enlarged by $\sqrt{l}$ times as the topological charge enlarges l times, which demonstrates that the generated vortex RFL satisfies the universal physical laws of the vortex beam. It is worth noting that, on the left of circular zone centrally located at interference image, there exists a mirror shape with nearly the same size and a fork fringe. This is owing to the double-faced reflection of the reflective mirror employed in the interferometer. As l is increased twofold corresponding to Fig. 5, the left

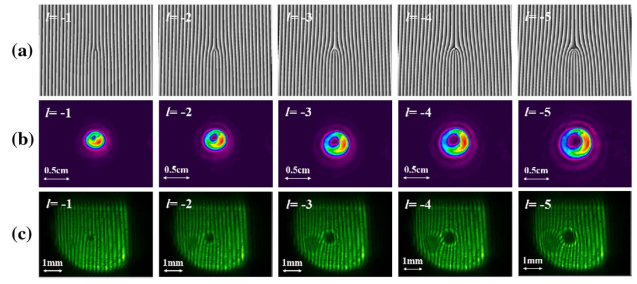

Fig. 4. (a) Holograms loaded onto the SLM. (b) Intensity distribution. (c) Interference fringes of the vortex RFL acquired by a CCD. The topological charge l is −5 to −1 from left to right.

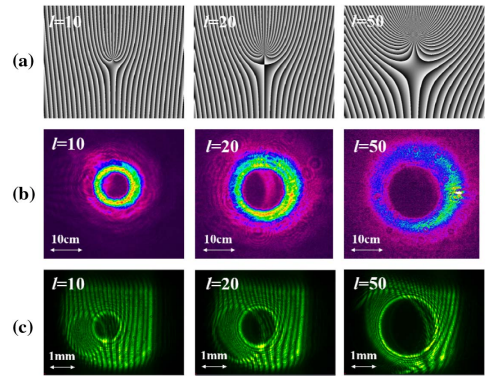

Fig. 5. (a) Holograms loaded onto the SLM. (b) Intensity distribution. (c) Interference fringes of the vortex RFL acquired by a CCD. The topological charge l is 10, 20, and 50 from left to right.

reflection image is displayed out of shape, resulting in a low visibility of characteristic interference fringes. The double-faced reflection is mainly due to two unparallel interfering light beams. Through adjustment of position and flip angle of the reflective mirror, the increased angle between the two light paths approaches zero, and the two circles centrally superpose.

A vortex RFL with fractional OAMs has been further demonstrated. Vortex profiles with topological charge l of 1.5 and 2.5 are shown in Fig. 6(b), which degenerate from complete circles to distorted hollow rings with a radial gap along the horizontal direction. The extent of the radial gap is large with half-integral topological numbers. Meanwhile, a serrated gap occurs connected with the circular zone horizontally, the size of which increases along with the growth of l, as shown in Fig. 6(c).

In fact, apart from the SLM, there are many other devices that can achieve vortex conversion, such as the spiral phase plate (SPP) and the mode-selective coupler (MSC). The SPP is widely applied in the generation of a vortex beam [49–53] with the advantages of convenient operation and high-power affordability. The MSC allows an all-fiber structure of the vortex beam generation [54–57] by virtue of operation stability, low intermode crosstalk, and rapid response rate. However, these two modulators are confined to single-functionality, which means that, for one wavelength, vortex beams can be generated only with a single topological charge, making it difficult to reach large topological charges. In this work, generation and verification of the vortex RFL are in demand for the extensible control of the topological charge and real-time monitoring of vortex beam. From our perspective, the SLM, which can realize dynamically controllable vortex beams with flexible operation, high control precision, and high resolution, is a preferable option among various modulators of vortex conversion.

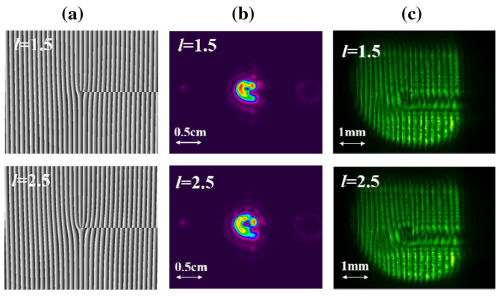

Fig. 6. (a) Holograms loaded onto the SLM. (b) Intensity distribution. (c) Interference fringes of vortex RFL acquired by a CCD. The topological charge l is 1.5 and 2.5 from left to right.

4. CONCLUSION

In summary, a vortex RFL with controllable OAM mode is successfully developed and experimentally realized. The topological charge of the vortex beam can range from −50 to 50 with nearly watt-level output power, and the spiral wavefront distribution is verified by implementing a triangular toroidal interferometer for a generated random laser with special coherence property. The intensity distributions of vortex spots are extremely rounded and homogeneous, which reveal central dark hollows; further, helical wavefront behaviors can be distinguished as unambiguous fork shapes. Fractional vortex RFLs are also analyzed, indicating that the generated vortex RFL follows the same physical laws as common vortices. This work may not only offer a new approach to temporal modulation of vortex beams and optical field control of an RFL but also provide an alternative laser source for vortex beams to expand their application in imaging, sensing, and communication.

Funding. National Natural Science Foundation of China (61635005, 61905284); National Postdoctoral Program for Innovative Talents (BX20190063); Hunan Innovative Province Construction Project (2019RS3017).

Acknowledgment. We are grateful to T. Hou for his important help with this work.

Disclosures. The authors declare no conflicts of interest related to this paper.

REFERENCES

1. L. Allen, M. W. Beijersbergen, R. J. C. Spreeuw, and J. P. Woerdman, "Orbital angular momentum of light and the transformation of Laguerre-Gaussian laser modes," Phys. Rev. A **45**, 8185–8189 (1992).
2. A. M. Yao and M. J. Padgett, "Orbital angular momentum: origins, behavior and applications," Adv. Opt. Photon. **3**, 161–204 (2011).
3. M. R. Dennis, K. O'Holleran, and M. J. Padgett, "Singular optics: optical vortices and polarization singularities," Prog. Opt. **53**, 293–363 (2009).
4. Y. Shen, X. Wang, Z. Xie, C. Min, X. Fu, Q. Liu, M. Gong, and X. Yuan, "Optical vortices 30 years on: OAM manipulation from topological charge to multiple singularities," Light Sci. Appl. **8**, 90 (2019).
5. W. Zhang, K. Wei, D. Mao, H. Wang, F. Gao, L. Huang, T. Mei, and J. Zhao, "Generation of femtosecond optical vortex pulse in fiber based on an acoustically induced fiber grating," Opt. Lett. **42**, 454–457 (2017).
6. T. Wang, A. Yang, F. Shi, Y. Huang, J. Wen, and X. Zeng, "High-order mode lasing in all-FMF laser cavities," Photon. Res. **7**, 42–49 (2019).
7. B. Wang, W. Liu, M. Zhao, J. Wang, Y. Zhang, A. Chen, F. Guan, X. Liu, L. Shi, and J. Zi, "Generating optical vortex beams by momentum-space polarization vortices centred at bound states in the continuum," Nat. Photonics **14**, 623–628 (2020).
8. Y. Zhang, X. Yang, and J. Gao, "Orbital angular momentum transformation of optical vortex with aluminum metasurfaces," Sci. Rep. **9**, 9133 (2019).

9. S. Fu, T. Wang, and C. Gao, "Perfect optical vortex array with controllable diffraction order and topological charge," J. Opt. Soc. Am. A **33**, 1836–1842 (2016).
10. J. Zeng, R. Lin, X. Liu, C. Zhao, and Y. Cai, "Review on partially coherent vortex beams," Front. Optoelectron. **12**, 229–248 (2019).
11. A. E. Willner, H. Huang, Y. Yan, Y. Ren, N. Ahmed, G. Xie, C. Bao, L. Li, Y. Cao, Z. Zhao, J. Wang, M. P. J. Lavery, M. Tur, S. Ramachandran, A. F. Molisch, N. Ashrafi, and S. Ashrafi, "Optical communications using orbital angular momentum beams," Adv. Opt. Photon. **7**, 66–106 (2015).
12. J. Liu, S. Li, J. Du, C. Klitis, C. Du, Q. Mo, M. Sorel, S. Yu, X. Cai, and J. Wang, "Performance evaluation of analog signal transmission in an integrated optical vortex emitter to 3.6-km few-mode fiber system," Opt. Lett. **41**, 1969–1972 (2016).
13. D. G. Grier, "A revolution in optical manipulation," Nature **424**, 810–816 (2003).
14. D. M. Palacios, I. D. Maleev, A. S. Marathay, and G. A. Swartzlander, "Spatial correlation singularity of a vortex field," Phys. Rev. Lett. **92**, 143905 (2004).
15. J. Peřina and Z. Bouchal, "Non-diffracting beams with controlled spatial coherence," J. Mod. Opt. **49**, 1673–1689 (2002).
16. M. Dong, D. Jiang, N. Luo, and Y. Yang, "Trapping two types of Rayleigh particles using a focused partially coherent anomalous vortex beam," Appl. Phys. B **125**, 55 (2019).
17. J. Yu, Y. Huang, F. Wang, X. Liu, G. Gbur, and Y. Cai, "Scintillation properties of a partially coherent vector beam with vortex phase in turbulent atmosphere," Opt. Express **27**, 26676–26688 (2019).
18. N. Bozinovic, Y. Yue, Y. Ren, M. Tur, P. Kristensen, H. Huang, A. E. Willner, and S. Ramachandran, "Terabit-scale orbital angular momentum mode division multiplexing in fibers," Science **340**, 1545–1548 (2013).
19. J. Liu, S.-M. Li, L. Zhu, A.-D. Wang, S. Chen, C. Klitis, C. Du, Q. Mo, M. Sorel, S.-Y. Yu, X.-L. Cai, and J. Wang, "Direct fiber vector eigenmode multiplexing transmission seeded by integrated optical vortex emitters," Light Sci. Appl. **7**, 17148 (2018).
20. D. Lin, J. Carpenter, Y. Feng, S. Jain, Y. Jung, Y. Feng, M. N. Zervas, and D. J. Richardson, "Reconfigurable structured light generation in a multicore fibre amplifier," Nat. Commun. **11**, 3986 (2020).
21. F. Brunet, Y. Taillon, P. Galarneau, and S. LaRochelle, "A simple model describing both self-mode locking and sustained self-pulsing in ytterbium-doped ring fiber lasers," J. Lightwave Technol. **23**, 2131–2138 (2005).
22. Y. Tang and J. Xu, "Effects of excited-state absorption on self-pulsing in Tm^{3+}-doped fiber lasers," J. Opt. Soc. Am. B **27**, 179–186 (2010).
23. J. Xu, Z. Lou, J. Ye, J. Wu, J. Leng, H. Xiao, H. Zhang, and P. Zhou, "Incoherently pumped high-power linearly-polarized single-mode random fiber laser: experimental investigations and theoretical prospects," Opt. Express **25**, 5609–5617 (2017).
24. N. Jhajj, I. Larkin, E. W. Rosenthal, S. Zahedpour, J. K. Wahlstrand, and H. M. Milchberg, "Spatiotemporal optical vortices," Phys. Rev. X **6**, 031037 (2016).
25. S. W. Hancock, S. Zahedpour, A. Goffin, and H. M. Milchberg, "Free-space propagation of spatiotemporal optical vortices," Optica **6**, 1547–1553 (2019).
26. L. Rego, K. Dorney, N. Brooks, Q. Nguyen, C.-T. Liao, J. San Roman, D. Couch, A. Liu, E. Pisanty, M. Lewenstein, L. Plaja, H. Kapteyn, M. Murnane, and C. Hernández-García, "Generation of extreme-ultraviolet beams with time-varying orbital angular momentum," Science **364**, eaaw9486 (2019).
27. A. Chong, C. Wan, J. Chen, and Q. Zhan, "Generation of spatiotemporal optical vortices with controllable transverse orbital angular momentum," Nat. Photonics **14**, 350–354 (2020).
28. S. K. Turitsyn, S. A. Babin, A. E. El-Taher, P. Harper, D. V. Churkin, S. I. Kablukov, J. D. Ania-Castañón, V. Karalekas, and E. V. Podivilov, "Random distributed feedback fibre laser," Nat. Photonics **4**, 231–235 (2010).
29. S. K. Turitsyn, S. A. Babin, D. V. Churkin, I. D. Vatnik, M. Nikulin, and E. V. Podivilov, "Random distributed feedback fibre lasers," Phys. Rep. **542**, 133–193 (2014).
30. P. Rosa, M. Tan, S. T. Le, I. D. Philips, J. D. Ania-Castañón, S. Sygletos, and P. Harper, "Unrepeatered DP-QPSK transmission over 352.8 km SMF using random DFB fiber laser amplification," IEEE Photon. Technol. Lett. **27**, 1189–1192 (2015).
31. M. Tan, P. Rosa, S. T. Le, M. A. Iqbal, I. Phillips, and P. Harper, "Transmission performance improvement using random DFB laser based Raman amplification and bidirectional second-order pumping," Opt. Express **24**, 2215–2221 (2016).
32. D. Leandro, V. deMiguel Soto, R. A. Perez-Herrera, M. B. Acha, and M. López-Amo, "Random DFB fiber laser for remote (200 km) sensor monitoring using hybrid WDM/TDM," J. Lightwave Technol. **34**, 4430–4436 (2016).
33. S. Rota-Rodrigo, B. Gouhier, C. Dixneuf, L. Antoni-Micollier, G. Guiraud, D. Leandro, M. Lopez-Amo, N. Traynor, and G. Santarelli, "Watt-level green random laser at 532 nm by SHG of a Yb-doped fiber laser," Opt. Lett. **43**, 4284–4287 (2018).
34. W. Pan, L. Zhang, H. Jiang, X. Yang, S. Cui, and Y. Feng, "Ultrafast Raman fiber laser with random distributed feedback," Laser Photon. Rev. **12**, 1700326 (2018).
35. Z. Wang, H. Wu, M. Fan, L. Zhang, Y. Rao, W. Zhang, and X. Jia, "High power random fiber laser with short cavity length: theoretical and experimental investigations," IEEE J. Sel. Top. Quantum Electron. **21**, 10–15 (2015).
36. H. Zhang, L. Huang, J. Song, H. Wu, P. Zhou, X. Wang, J. Wu, J. Xu, Z. Wang, X. Xu, and Y. Rao, "Quasi-kilowatt random fiber laser," Opt. Lett. **44**, 2613–2616 (2019).
37. Z. Wang, P. Yan, Y. Huang, J. Tian, C. Cai, D. Li, Y. Yi, Q. Xiao, and M. Gong, "An efficient 4-kW level random fiber laser based on a tandem-pumping scheme," IEEE Photon. Technol. Lett. **31**, 817–820 (2019).
38. J. Xu, L. Huang, M. Jiang, J. Ye, P. Ma, J. Leng, J. Wu, H. Zhang, and P. Zhou, "Near-diffraction-limited linearly polarized narrow-linewidth random fiber laser with record kilowatt output," Photon. Res. **5**, 350–354 (2017).
39. E. A. Zlobina, S. I. Kablukov, and S. A. Babin, "Linearly polarized random fiber laser with ultimate efficiency," Opt. Lett. **40**, 4074–4077 (2015).
40. Z. Hu, R. Ma, X. Zhang, Z. Sun, X. Liu, J. Liu, K. Xie, and L. Zhang, "Weak feedback assisted random fiber laser from 45°-tilted fiber Bragg grating," Opt. Express **27**, 3255–3263 (2019).
41. V. Balaswamy, S. Aparanji, S. Arun, S. Ramachandran, and V. R. Supradeepa, "High-power, widely wavelength tunable, grating-free Raman fiber laser based on filtered feedback," Opt. Lett. **44**, 279–282 (2019).
42. J. Ye, Y. Zhang, J. Xu, J. Song, T. Yao, H. Xiao, J. Leng, and P. Zhou, "Broadband pumping enabled flat-amplitude multi-wavelength random Raman fiber laser," Opt. Lett. **45**, 1786–1789 (2020).
43. X. Jin, Z. Lou, H. Zhang, J. Xu, P. Zhou, and Z. Liu, "Random distributed feedback fiber laser at 2.1 μm," Opt. Lett. **41**, 4923–4926 (2016).
44. X. P. Zeng, W. L. Zhang, R. Ma, Z. J. Yang, X. Zeng, X. Dong, and Y. J. Rao, "Regulation of a pulsed random fiber laser in the *Q*-switched regime," Laser Phys. Lett. **13**, 115105 (2016).
45. J. Xu, J. Ye, W. Liu, J. Wu, H. Zhang, J. Leng, and P. Zhou, "Passively spatiotemporal gain-modulation-induced stable pulsing operation of a random fiber laser," Photon. Res. **5**, 598–603 (2017).
46. R. Ma, Y. J. Rao, W. L. Zhang, and B. Hu, "Multimode random fiber laser for speckle-free imaging," IEEE J. Sel. Top. Quantum Electron. **25**, 2833472 (2019).
47. B. Redding, M. A. Choma, and H. Cao, "Speckle-free laser imaging using random laser illumination," Nat. Photonics **6**, 355–359 (2012).
48. S. Sugavanam, M. Sorokina, and D. V. Churkin, "Spectral correlations in a random distributed feedback fibre laser," Nat. Commun. **8**, 15514 (2017).
49. M. W. Beijersbergen, R. P. C. Coerwinkel, M. Kristensen, and J. P. Woerdman, "Helical-wavefront laser beams produced with a spiral phaseplate," Opt. Commun. **112**, 321–327 (1994).
50. Y. Shen, G. T. Campbell, B. Hage, H. Zou, B. C. Buchler, and P. K. Lam, "Generation and interferometric analysis of high charge optical vortices," J. Opt. **15**, 044005 (2013).
51. W. Huang, J. Li, H. Wang, J. Wang, and S. Gao, "Vortex electromagnetic waves generated by using a laddered spiral phase plate and a microstrip antenna," Electromagnetics **36**, 102–110 (2016).

52. C. Wang, T. Liu, Y. Ren, Q. Shao, and H. Dong, "Generating optical vortex with large topological charges by spiral phase plates in cascaded and double-pass configuration," Optik **171**, 404–412 (2018).
53. S. N. Khonina, A. V. Ustinov, V. I. Logachev, and A. P. Porfirev, "Properties of vortex light fields generated by generalized spiral phase plates," Phys. Rev. A **101**, 043829 (2020).
54. M. S. Whalen and T. H. Wood, "Effectively nonreciprocal evanescent-wave optical-fibre directional coupler," Electron. Lett. **21**, 175–176 (1985).
55. T. Wang, F. Wang, F. Shi, F. Pang, S. Huang, T. Wang, and X. Zeng, "Generation of femtosecond optical vortex beams in all-fiber mode-locked fiber laser using mode selective coupler," J. Lightwave Technol. **35**, 2161–2166 (2017).
56. H. Wan, J. Wang, Z. Zhang, Y. Cai, B. Sun, and L. Zhang, "High efficiency mode-locked, cylindrical vector beam fiber laser based on a mode selective coupler," Opt. Express **25**, 11444–11451 (2017).
57. C. Dong, J. Zou, H. Wang, H. Yao, X. Zeng, Y. Bu, and Z. Luo, "Visible-light all-fiber vortex lasers based on mode selective couplers," Chin. Phys. B **29**, 094204 (2020).